

# Transition of recollision trajectories from linear to elliptical polarization

Yingbin Li,<sup>1,2</sup> Benhai Yu,<sup>3,8</sup> Qingbin Tang,<sup>3</sup> Xu Wang,<sup>4,9</sup> Duanyang Hua,<sup>3</sup> Aihong Tong,<sup>5</sup>  
Chenghuan Jiang,<sup>1,2,6</sup> Guixian Ge,<sup>1,7</sup> Yongchao Li,<sup>1,2</sup> and Jianguo Wan<sup>1,2,10</sup>

<sup>1</sup>National Laboratory of Solid State Microstructures and Department of Physics, Nanjing University, Nanjing 210093, China

<sup>2</sup>Collaborative Innovation Center of Advanced Microstructures, Nanjing University, Nanjing 210093, China

<sup>3</sup>College of physics and Electronic Engineering, Xinyang Normal University, Xinyang 464000, China

<sup>4</sup>Department of Physics, Kansas State University, Manhattan, KS 66506, USA

<sup>5</sup>Department of Physics and Mechanical and Electrical Engineering, Hubei University of Education, Wuhan 430205, China

<sup>6</sup>Institute of Communication and Technology, Communication University, Nanjing 211172, China

<sup>7</sup>Key Laboratory of Ecophysics and Department of Physics, College of Science, Shihezi University, Xinjiang 832003, China

<sup>8</sup>hnyubenhai@163.com

<sup>9</sup>xuwang@phys.ksu.edu

<sup>10</sup>wanjj@nju.edu.cn

**Abstract:** Using a classical ensemble method, we revisit the topic of recollision and nonsequential double ionization with elliptically polarized laser fields. We focus on how the recollision mechanism transitions from short trajectories with linear polarization to long trajectories with elliptical polarization. We propose how this transition can be observed by measuring the carrier-envelope-phase dependence of the correlated electron momentum spectra using currently available few-cycle laser pulses.

©2016 Optical Society of America

**OCIS codes:** (020.4180) Multiphoton processes; (260.3230) Ionization; (270.6620) Strong-field process.

---

## References and links

1. W. Becker, X. Liu, P. J. Ho, and J. H. Eberly, "Theories of photoelectron correlation in laser-driven multiple atomic ionization," *Rev. Mod. Phys.* **84**(3), 1011–1043 (2012).
2. D. N. Fittinghoff, P. R. Bolton, B. Chang, and K. C. Kulander, "Observation of nonsequential double ionization of helium with optical tunneling," *Phys. Rev. Lett.* **69**(18), 2642–2645 (1992).
3. B. Walker, B. Sheehy, L. F. DiMauro, P. Agostini, K. J. Schafer, and K. C. Kulander, "Precision measurement of strong field double ionization of helium," *Phys. Rev. Lett.* **73**(9), 1227–1230 (1994).
4. K. C. Kulander, K. J. Schafer, and J. L. Krause, *Dynamics of Short-Pulse Excitation, Ionization and Harmonic Conversion*, in *Super-Intense Laser-Atom Physics*, edited by B. Piraux, A. L'Huillier, and K. Rzazewski (Plenum, New York, 1993).
5. K. J. Schafer, B. Yang, L. F. DiMauro, and K. C. Kulander, "Intensity-dependent scattering rings in high order above-threshold ionization," *Phys. Rev. Lett.* **70**, 1599 (1993).
6. P. B. Corkum, "Plasma perspective on strong field multiphoton ionization," *Phys. Rev. Lett.* **71**(13), 1994–1997 (1993).
7. P. Dietrich, N. H. Burnett, M. Ivanov, and P. B. Corkum, "High-harmonic generation and correlated two-electron multiphoton ionization with elliptically polarized light," *Phys. Rev. A* **50**(5), R3585–R3588 (1994).
8. N. H. Burnett, C. Kan, and P. B. Corkum, "Ellipticity and polarization effects in harmonic generation in ionizing neon," *Phys. Rev. A* **51**(5), R3418–R3421 (1995).
9. G. D. Gillen, M. A. Walker, and L. D. VanWoerkom, "Enhanced double ionization with circularly polarized light," *Phys. Rev. A* **64**(4), 043413 (2001).
10. C. Guo and G. N. Gibson, "Ellipticity effects on single and double ionization of diatomic molecules in strong laser fields," *Phys. Rev. A* **63**(4), 040701 (2001).
11. C. Guo, M. Li, J. P. Nibarger, and G. N. Gibson, "Single and double ionization of diatomic molecules in strong laser fields," *Phys. Rev. A* **58**(6), R4271–R4274 (1998).
12. N. I. Shvetov-Shilovski, S. P. Goreslavski, S. V. Popruzhenko, and W. Becker, "Ellipticity effects and the contributions of long orbits in nonsequential double ionization of atoms," *Phys. Rev. A* **77**(6), 063405 (2008).
13. X. Wang and J. H. Eberly, "Elliptical trajectories in nonsequential double ionization," *New J. Phys.* **12**(9), 093047 (2010).
14. X. Wang and J. H. Eberly, "Elliptical polarization and probability of double ionization," *Phys. Rev. Lett.* **105**(8), 083001 (2010).

15. F. Mauger, C. Chandre, and T. Uzer, "Recollisions and correlated double ionization with circularly polarized light," *Phys. Rev. Lett.* **105**(8), 083002 (2010).
16. L. B. Fu, G. G. Xin, D. F. Ye, and J. Liu, "Recollision dynamics and phase diagram for nonsequential double ionization with circularly polarized laser fields," *Phys. Rev. Lett.* **108**(10), 103601 (2012).
17. A. Kamor, F. Mauger, C. Chandre, and T. Uzer, "How key periodic orbits drive recollisions in a circularly polarized laser field," *Phys. Rev. Lett.* **110**(25), 253002 (2013).
18. J. Guo, X. Liu, and S. I. Chu, "Exploration of nonsequential-double-ionization dynamics of Mg atoms in linearly and circularly polarized laser fields with different potentials," *Phys. Rev. A* **88**(2), 023405 (2013).
19. X. Lai, C. Wang, Y. Chen, Z. Hu, W. Quan, X. Liu, J. Chen, Y. Cheng, Z. Xu, and W. Becker, "Elliptical polarization favors long quantum orbits in high-order above-threshold ionization of noble gases," *Phys. Rev. Lett.* **110**(4), 043002 (2013).
20. Y. Zhou, C. Huang, Q. Liao, and P. Lu, "Classical simulations including electron correlations for sequential double ionization," *Phys. Rev. Lett.* **109**(5), 053004 (2012).
21. P. J. Ho, R. Panfili, S. L. Haan, and J. H. Eberly, "Nonsequential double ionization as a completely classical photoelectric effect," *Phys. Rev. Lett.* **94**(9), 093002 (2005).
22. S. L. Haan, J. S. Van Dyke, and Z. S. Smith, "Recollision excitation, electron correlation, and the production of high-momentum electrons in double ionization," *Phys. Rev. Lett.* **101**(11), 113001 (2008).
23. A. Tong, Y. Zhou, and P. Lu, "Resolving subcycle electron emission in strong-field sequential double ionization," *Opt. Express* **23**(12), 15774–15783 (2015).
24. T. Weber, H. Giessen, M. Weckenbrock, G. Urbasch, A. Staudte, L. Spielberger, O. Jagutzki, V. Mergel, M. Vollmer, and R. Dörner, "Correlated electron emission in multiphoton double ionization," *Nature* **405**(6787), 658–661 (2000).
25. A. Staudte, C. Ruiz, M. Schöffler, S. Schössler, D. Zeidler, T. Weber, M. Meckel, D. M. Villeneuve, P. B. Corkum, A. Becker, and R. Dörner, "Binary and recoil collisions in strong field double ionization of helium," *Phys. Rev. Lett.* **99**(26), 263002 (2007).
26. A. Rudenko, V. L. B. de Jesus, T. Ergler, K. Zrost, B. Feuerstein, C. D. Schröter, R. Moshhammer, and J. Ullrich, "Correlated two-electron momentum spectra for strong-field nonsequential double ionization of He at 800 nm," *Phys. Rev. Lett.* **99**(26), 263003 (2007).
27. D. F. Ye, X. Liu, and J. Liu, "Classical trajectory diagnosis of a fingerlike pattern in the correlated electron momentum distribution in strong field double ionization of helium," *Phys. Rev. Lett.* **101**(23), 233003 (2008).
28. J. S. Parker, L. R. Moore, D. Dundas, and K. T. Taylor, "Double ionization of helium at 390 nm," *J. Phys. B* **33**(20), L691–L698 (2000).
29. S. X. Hu, "Boosting photoabsorption by attosecond control of electron correlation," *Phys. Rev. Lett.* **111**(12), 123003 (2013).
30. A. Liu and U. Thumm, "Laser-assisted XUV few-photon double ionization of helium: Joint angular distributions," *Phys. Rev. A* **89**(6), 063423 (2014).
31. R. Panfili, J. Eberly, and S. Haan, "Comparing classical and quantum simulations of strong-field double-ionization," *Opt. Express* **8**(7), 431–435 (2001).
32. R. Panfili, S. L. Haan, and J. H. Eberly, "Slow-down collisions and nonsequential double ionization in classical simulations," *Phys. Rev. Lett.* **89**(11), 113001 (2002).
33. J. Javanainen, J. H. Eberly, and Q. Su, "Numerical simulations of multiphoton ionization and above-threshold electron spectra," *Phys. Rev. A* **38**(7), 3430–3446 (1988).
34. Q. Su and J. H. Eberly, "Model atom for multiphoton physics," *Phys. Rev. A* **44**(9), 5997–6008 (1991).
35. X. Wang, J. Tian, and J. H. Eberly, "Angular correlation in strong-field double ionization under circular polarization," *Phys. Rev. Lett.* **110**(7), 073001 (2013).
36. B. Bergues, M. Kübel, N. G. Johnson, B. Fischer, N. Camus, K. J. Betsch, O. Herrwerth, A. Senftleben, A. M. Saylor, T. Rathje, T. Pfeifer, I. Ben-Itzhak, R. R. Jones, G. G. Paulus, F. Krausz, R. Moshhammer, J. Ullrich, and M. F. Kling, "Attosecond tracing of correlated electron-emission in non-sequential double ionization," *Nat. Commun.* **3**, 813 (2012).
37. N. Camus, B. Fischer, M. Kremer, V. Sharma, A. Rudenko, B. Bergues, M. Kübel, N. G. Johnson, M. F. Kling, T. Pfeifer, J. Ullrich, and R. Moshhammer, "Attosecond correlated dynamics of two electrons passing through a transition state," *Phys. Rev. Lett.* **108**(7), 073003 (2012).
38. S. L. Haan, Z. S. Smith, K. N. Shomsky, P. W. Plantinga, and T. L. Atallah, "Anticorrelated electrons from high-intensity nonsequential double ionization of atoms," *Phys. Rev. A* **81**(2), 023409 (2010).

---

## 1. Introduction

A tremendous amount of theoretical efforts [for a review, see 1] have been devoted to strong-field ionization during the past two decades since the discovery of nonsequential double ionization (NSDI) [2, 3], which has been regarded as one of the most prominent manifests of electron-electron correlation in Nature. The measured atomic double ionization (DI) yields can be many orders of magnitude higher than the predicted yields assuming sequential, or independent, release of the two emitted electrons.

NSDI can be well understood from a semiclassical recollision scenario [4–6]: First, one electron is emitted via tunneling through the laser-tilted Coulomb potential barrier and is driven away from its parent ion core; Second, as the oscillating laser electric field reverses its

direction, the first-emitted electron can be driven back to recollide with its parent ion core and kick out a second electron, leading to nonsequential or correlated emission of two electrons.

From this simple yet intuitive recollision scenario, it is obvious to see that recollision and NSDI depend critically on the polarization of the external laser field. If the laser field is elliptically or circularly polarized, then the probability of recollision is greatly reduced or even completely eliminated because the additional field along the transverse direction steers away the first-emitted electron, reducing or eliminating its chance of returning to the parent ion core. This point was indeed supported by some early experiments with elliptical polarization on rare gas targets such as Ar and Ne [7, 8]. However, and interestingly, later experiments reported characteristic NSDI events with atomic target Mg [9] and with some molecular targets such as NO and O<sub>2</sub> even with circularly polarized laser fields [10, 11], reinitiating interest to this once-believed-settled topic.

Substantial theoretical efforts have been devoted to understanding the mechanism of NSDI with elliptical or circular polarization and the apparent species dependency [12–18]. It has been conjectured that recollision is still the mechanism responsible for the observed NSDI characteristics with elliptical or circular polarization and that recollision is possible with elliptical polarization via a family of recollisional “elliptical trajectories” [13], the chance for which to happen depends critically on the atomic or molecular species [15, 16]. A demonstration of the conjectured recollision trajectory with elliptical polarization (EP) is shown in Fig. 1(a) and its distinction from a typical recollision trajectory with linear polarization (LP), as illustrated in Fig. 1(b), is obvious. For LP, if an electron is emitted to the

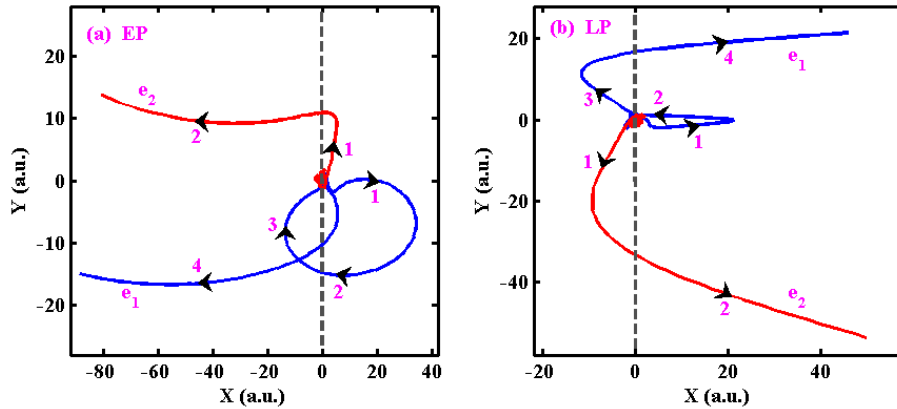


Fig. 1. Demonstration of typical recollision trajectories with EP (a) and with LP (b). The trajectory of the first-emitted electron is shown in blue and the trajectory of the second-emitted electron is shown in red. The arrows and numbers are used to show the temporal motion of the two electrons.

+ x direction, it usually will return from the + x direction and kick out a second electron to the -x direction. Whereas for EP, if an electron is emitted to the + x direction, it usually will circle around the parent ion core, return from the -x direction and kick out a second electron to the + x direction. Although more complicated recollision trajectories do exist for both LP and EP, as will be shown later in this paper, the two trajectories shown in Fig. 1 are the most typical and dominant ones for EP or LP.

The trajectory shown in Fig. 1(b) for LP is a typical “short” trajectory and the one shown in Fig. 1(a) for EP is a typical “long” trajectory, which can be distinguished by the criterion whether the first-emitted electron recollides the first time it passes through the plane  $x = 0$  [12]. In the context of single ionization, the relative contribution of short and long trajectories as a function of laser field ellipticity has been studied experimentally by Lai *et al.* [19].

In this paper, we study the transition from short-trajectory-dominant recollision with LP to long-trajectory-dominant recollision with EP, using a classical ensemble method that has been

widely used previously to study strong-field DI processes [13–18, 20–23]. We analyze the relative contributions of short and long recollision trajectories and show their transitions from LP to EP. We predict that this transition manifests itself in correlated electron momentum spectra [24–27] if few-cycle carrier-envelope phase (CEP) stabilized laser pulses are used, which are readily available in many laboratories around the world, therefore this transition can be directly observed in experiments.

This paper is organized as follows. In Section 2 we give a brief introduction to the classical ensemble method that we use to do the calculation. Numerical results and detailed analyses and discussions are presented in Section 3. A conclusion is given in Section 4.

## 2. Method

Atoms are fundamentally quantum mechanical systems therefore the interaction between an atom and an external laser field is described by the corresponding multi-electron time-dependent Schrödinger equation. However, the computational load of calculating a multi-electron system in a strong laser field is extremely demanding and attempts along this line [28–30] have been limited to the He atom, usually with reduced experimental conditions. There is no near-future perspective of extending *ab initio* strong-field calculations to atoms beyond the He atom, such as Ar, Ne, Xe, etc., on which most current experiments are performed.

An alternative classical ensemble method was proposed by Eberly and associates [31, 32] and has been widely used to describe strong-field double ionization processes qualitatively or semi-quantitatively [13–18, 20–23]. The general idea is to mimic a quantum mechanical wavefunction using an ensemble of classically modeled atoms. Compared to *ab initio* quantum mechanical calculations, the classical ensemble method requires little computational resource and can be performed very quickly. Another important advantage of the classical ensemble method is trajectory back analysis: calculation outcomes of interest can be back-analyzed to gain direct insight of the involved physical processes.

Since detailed introductions and tests have been given previously [31, 32], here we only give a brief description of the method. In this fully classical model, the evolution of a two-electron system is governed by the Newtonian equation of motion (atomic units are used throughout this paper unless otherwise stated):

$$d^2 \mathbf{r}_i / dt^2 = -\nabla[V_{ne}(\mathbf{r}_i) + V_{ee}(\mathbf{r}_{ij})] - E(t), \quad (1)$$

where  $\mathbf{r}_i$  is the position vector of the  $i$ -th electron,  $V_{ne}$  and  $V_{ee}$  are the nuclear-electron and electron-electron Coulomb potential, respectively, and  $E(t)$  is the time-dependent laser electric field. In this paper, we use two few-cycle laser pulses, one linearly polarized and the other elliptically polarized. For the latter case, the polarization lies in the x-y plane, and the total electric field  $E(t)$  can be divided into two components:

$$\begin{aligned} E_x &= (E_0 / \sqrt{\varepsilon^2 + 1}) f(t) \sin(\omega t + \Phi), \\ E_y &= (\varepsilon E_0 / \sqrt{\varepsilon^2 + 1}) f(t) \cos(\omega t + \Phi), \end{aligned} \quad (2)$$

where  $E_0$ ,  $\varepsilon$ ,  $\omega$ , and  $\Phi$  are the amplitude, degree of ellipticity, angular frequency, and CEP, respectively. For EP, the x-axis is chosen as the major axis and the y-axis as the minor axis. For LP, we put  $\varepsilon = 0$  and the laser field is along the x-axis only. The function  $f(t)$  is the pulse envelope, given below:

$$f(t) = \sin^2 \left( \frac{\pi t}{NT} \right), \quad (3)$$

where  $T$  is the laser period and  $N$  is the number of laser cycles in the pulse.

The nuclear-electron and electron-electron Coulomb potentials are given by

$$V_{ne}(r_i) = -2 / \sqrt{|r_i|^2 + a^2}, \text{ and } V_{ee}(r_1, r_2) = 1 / \sqrt{|r_1 - r_2|^2 + b^2}, \quad (4)$$

respectively. To avoid the effect of autoionization when modeling a two-electron atom classically, we have used a soft-core Coulomb potential [33,34] with screening parameter  $a = 2.0$  a.u. For the electron-electron potential, we set  $b = 0.1$  a.u. to avoid singularities in numerical integration [35].

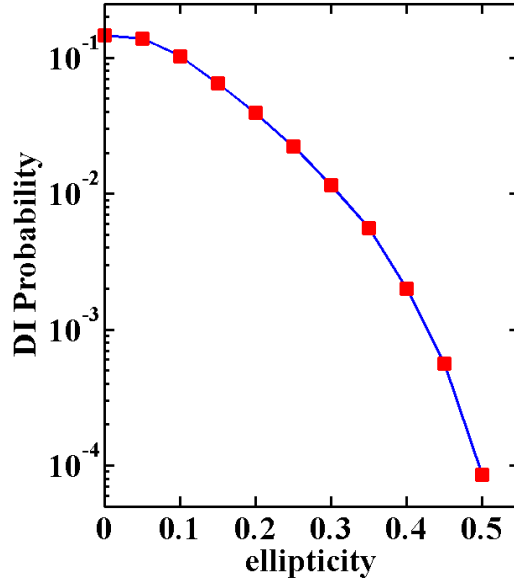


Fig. 2. Probability of double ionization as a function of ellipticity, for an intensity of  $2.5 \times 10^{14}$  W/cm<sup>2</sup> and a 6-cycle  $\sin^2$  pulse.

The initial ensemble before applying the laser electric field is populated within the classically allowed region for energy  $E_{tot} = -1.23$  a.u., which is set to be the negative sum of the first two ionization energies of the Xe atom (12.13eV and 20.98eV, respectively). For each model atom, the positions of the two electrons are first assigned randomly within the classically allowed region. The remaining energy (the total two-electron energy minus the total potential energy with the assigned electron positions) is the total kinetic energy of the two electrons and is randomly partitioned to each electron. Given a kinetic energy, the direction of the momentum is randomly assigned. The initial ensemble is populated with a large number of such model atoms, each with the same total energy but randomly assigned electron configurations. The size of the ensemble (i.e., the number of model atoms) is  $2.0 \times 10^5$  for LP and  $2.0 \times 10^6$  for EP. The reason to use a larger ensemble for EP is because the probability of getting DI is lower for EP. As shown in Fig. 2, for example, the probability of DI for ellipticity 0.3 is about an order of magnitude lower than that for LP, for an intensity of  $2.5 \times 10^{14}$  W/cm<sup>2</sup> and a 6-cycle  $\sin^2$  pulse.

In our calculation, for EP we choose  $\varepsilon = 0.3$ . As will be shown in Section III, this ellipticity value is large enough to suppress short recollision trajectories that dominate LP and at the same time small enough to obtain enough DI events for subsequent statistical analyses. With a higher ellipticity value, the probability of getting DI will be lower thus statistics will not be as good, but the main recollision physics will be the same.

After the initial ensemble is generated, we turn on the external laser electric field. Each model atom in the ensemble will interact with the laser field and the motion of the two electrons is determined by the classical Newtonian equation of motion given in Eq. (1). If the

laser field is strong enough, one or two electrons may be pulled out by the laser field from the atom yielding single ionization or double ionization. Statistics, e.g., probability of DI of the ensemble, can be analyzed after the laser pulse is over. In this paper, we define a DI event if the energies of both electrons of a model atom are positive at the end of pulse.

Positions and momenta of the two electrons can be monitored throughout the time duration of the laser pulse. At the end of the pulse correlated electron momentum spectra can be recorded which contain information about ionization dynamics that is not available otherwise.

### 3. Results and discussions

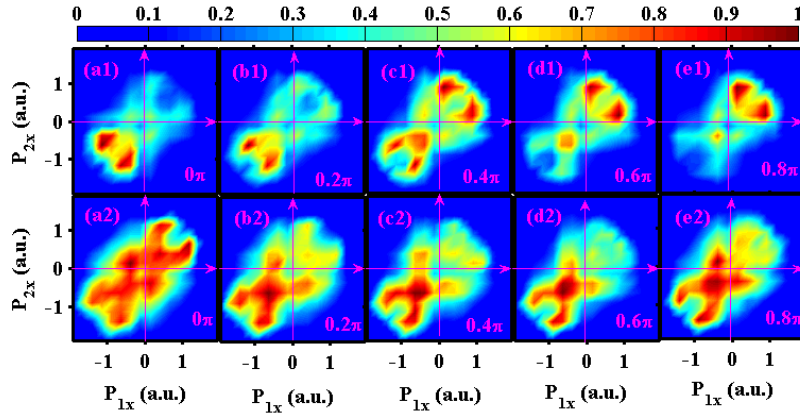


Fig. 3. Correlated electron momentum spectra along the x direction (i.e.,  $P_{1x}$  vs.  $P_{2x}$ ) for LP (upper row) and for EP (bottom row) under five different CEPs, as labeled on the lower right corner of each panel. The two rows are obtained with the same laser parameters except the ellipticity value. The laser intensity and wavelength are  $2.5 \times 10^{14}$  W/cm<sup>2</sup> and 780 nm, respectively.

Figure 3 shows correlated electron momentum spectra along the x direction ( $P_{1x}$  vs.  $P_{2x}$ ) for LP (upper row) and for EP (bottom row) under five different CEPs, as labeled on each panel. All laser parameters for LP and EP are the same except for the value of  $\varepsilon$  in Eq. (2). One can see that for each CEP, the momentum correlation between the two emitted electrons changes substantially when the laser field ellipticity changes from LP to EP. For example, for CEP = 0 (the leftmost column) and with LP, the majority of the population is in the third quadrant with  $P_{1x} < 0$  and  $P_{2x} < 0$ , meaning that both electrons are moving to the  $-x$  direction after recollision. Whereas with EP, much population moves to the first quadrant, which corresponds to both electrons moving to the  $+x$  direction after recollision. A minor portion of population is also found in the second and the fourth quadrants, corresponding to one electron moving to the  $+x$  direction and the other moving to the  $-x$  direction after recollision. We mention that the calculated spectra in the upper row for LP are similar in shape to the experimental data reported in [36, 37], even though a different atomic target (Ar) was used in these experiments.

It is also interesting to make a comparison between the e-e correlation spectra shown above and the ones obtained by the strong field approximation (SFA), e.g., Figs. 6 and 7 in [12], which does not include the ion core Coulomb attraction and assumes a three-body contact interaction, instead of the correct long-range Coulomb repulsion, for the e-e collision. The spectra obtained by SFA have no population in the second and the fourth quadrants, and do not reproduce the so-called V-shaped structure (also called the fingerlike structure) shown in the first and the third quadrants observed in experiments [25–27]. The inclusion of the ion core Coulomb attraction is responsible for the population in the second and the fourth quadrants, and the inclusion of Coulomb e-e repulsion is responsible for the V-shaped structure in the first and the third quadrants.

The change of correlated electron momentum distribution from LP to EP is a clear manifestation of the transition of recollision processes from short-trajectory dominant to long-trajectory dominant, as illustrated in Fig. 1. Therefore correlated electron momentum spectra provide a direct observation of recollision mechanism, and this information is not available otherwise from integrated quantities, such as the total DI yield.

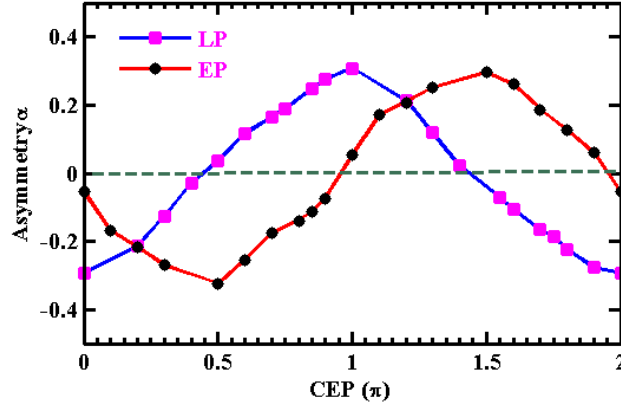


Fig. 4. Asymmetry parameter  $\alpha$  for LP and for EP under different carrier-envelope phases from 0 to  $2\pi$ .

To be more quantitative, we define an asymmetry parameter  $\alpha$ , similar to the one defined in [12]:

$$\alpha = \frac{W_{+x} - W_{-x}}{W_{+x} + W_{-x}} \quad (5)$$

where  $W_{+x}$  ( $W_{-x}$ ) is the population (i.e., number of electron pairs) in the first (third) quadrant. This  $\alpha$  parameter directly reflects the directionality of the recollision process. If all the population is in the first quadrant (both electrons moving to  $+x$ ), then  $\alpha = 1$ ; if all the population is in the third quadrant (both electrons moving to  $-x$ ), then  $\alpha = -1$ . Otherwise in general,  $\alpha$  lies in between these two limiting values and is a measure of the directionality of the recollision process.

The  $\alpha$  parameters corresponding to Fig. 3 are shown in Fig. 4, including more CEPs between 0 and  $2\pi$ . One sees that for each CEP, the asymmetry parameter  $\alpha$  changes substantially from LP to ellipticity 0.3. And for both LP and EP, the parameter  $\alpha$  oscillates between two limits with opposite signs. For the laser parameters used in our calculation, the maximum asymmetry value is about 0.3, for both LP and EP.

Figures 3 and 4 can be measured experimentally and such measurements can provide valuable insights about the DI recollision dynamics and how this dynamics changes with the ellipticity of the laser field. To gain a deeper understanding about the transition of recollision trajectory from LP to EP by taking the advantage of trajectory back analysis, we post-select all doubly ionized model atoms and perform a back analysis for each of them, recording the time of first ionization ( $t_{i1}$ ) and the time of recollision ( $t_r$ ). Here  $t_{i1}$  is defined as the time when the energy of the first emitted electron (including the kinetic energy, the ion-electron potential energy and half of the electron-electron potential energy) just becomes positive. The recollision time  $t_r$  is defined as the time of closest approach between the two electrons after the departure of the first electron.

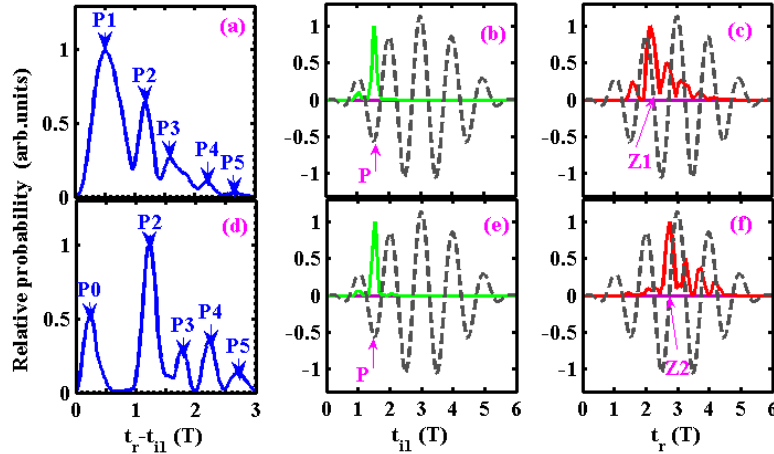


Fig. 5. Statistical distributions of the first ionization time  $t_{ii}$  (middle column), the recollision time  $t_r$  (right column), and their difference  $t_r - t_{ii}$  (left column) for LP (upper row) and for EP (bottom row).

Figure 5 shows the statistical analysis of  $t_{ii}$ ,  $t_r$ , and  $t_r - t_{ii}$ , for LP (upper row) and EP (bottom row). Here we have chosen CEP  $\Phi = 0.5\pi$ , for both LP and EP. Figure 5(a) shows the distribution of the time difference  $t_r - t_{ii}$  for LP. We see that the most prominent contribution is from the peak labeled “P1”, at about 0.5 laser cycles, corresponding to the short recollision trajectories demonstrated in Fig. 1(b). Longer recollision trajectories do contribute, as shown by the peaks P2, P3, P4, and P5, although their importance decreases quickly as the time difference increases. In contrast, for EP, we see from Fig. 5(d) that the dominant contribution is from the long recollision trajectories labeled “P2”, corresponding to the trajectories demonstrated in Fig. 1(a). We notice that P2 is peaked at about 1T. The peak P1 that dominates LP is almost completely suppressed. Longer trajectories also contribute, such as P3, P4, and P5, with less importance though.

The statistical distributions of  $t_{ii}$  and  $t_r$  are shown in the right two columns of Fig. 5, along with the laser electric field profile along the major polarization direction (the x-direction). We see that for both LP and EP, the first electron is emitted almost at the same time, around the laser field peak labeled “P”. Whereas the recollision time is very different: the most probable recollision time for LP is about half a cycle later from the ionization of the first electron, labeled as “Z1” in Fig. 5(c); in contrast, the most probable recollision for EP is about one cycle later from the ionization of the first electron, labeled as “Z2” in Fig. 5(f).

Examples of even longer recollision trajectories than the one demonstrated in Fig. 1(a) are shown in Fig. 6, corresponding to the peaks P3 and P4 of Fig. 5(d), respectively. The first-emitted electron may not be “lucky enough” to find its parent ion core after one laser cycle, instead, it may need an additional half cycle, or full cycle to find its parent ion core and kick out a second electron. We mention that similar recollision trajectories have also been discussed in [13] by Wang and Eberly.

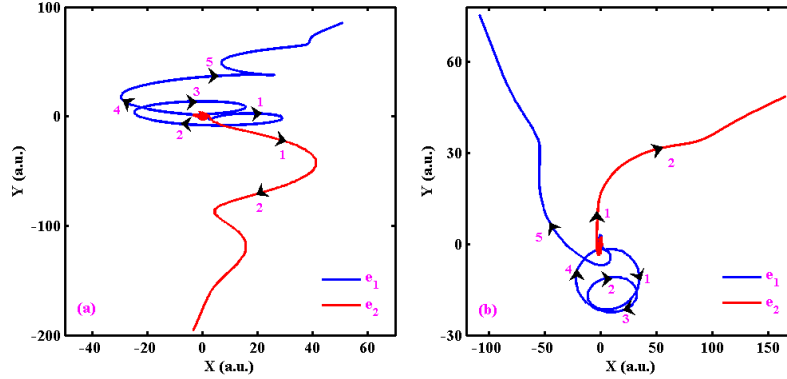


Fig. 6. Examples of “even longer” recollision trajectories for EP. The trajectory of the first-emitted electron is shown in blue and the trajectory of the second-emitted electron is shown in red. The arrows and numbers are used to show the temporal motion of the two electrons.

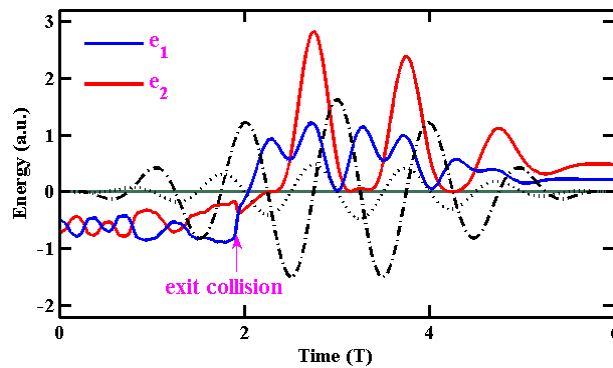


Fig. 7. Example of an exit-collision trajectory leading to DI. The energy trajectory of the first-emitted electron is shown in blue and that of the second-emitted electron is shown in red. Also shown is the electric field along the x-direction ( $E_x$ , dash-dot line) and along the y-direction ( $E_y$ , dotted line).

A special explanation is needed for the peak labeled “P0” in Fig. 5(d). P0 is located at 0.25T and we point out that this DI channel is not from recollision. Instead, it is from a DI channel called “exit collisions”, which has been discussed by Haan et al. with linearly polarized laser fields [38]. Figure 7 shows an example of an exit-collision trajectory. The energies of the two electrons (blue and red) are shown as a function of time, on top of the relative electric field strengths along the major direction ( $E_x$ ) and along the minor direction ( $E_y$ ). We can see that at time around 2T, when the field along the x-direction is maximum and the energies of both electrons are negative, the first (blue) electron is pulled out by the external laser field. On its way out, it gives part of its energy to the second (red) electron so that the second electron is highly excited after the first electron is out. This is in contrast to a typical first ionization where the emission of the first electron needs to borrow energy from the second electron. This exit collision excites the second electron so that the second electron can be ionized a quarter cycle later when the field along the y-direction is maximum. This is why P0 is peaked at 0.25T for EP.

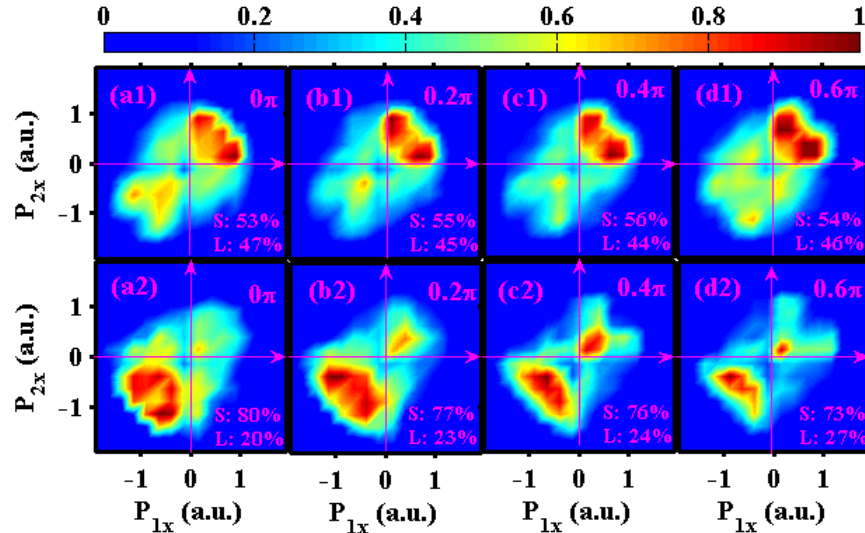


Fig. 8. Correlated electron momentum spectra along the x direction for 6-cycle (upper row) and for 4-cycle (bottom row) elliptically polarized laser pulses at intensity  $1.7 \times 10^{14}$  W/cm<sup>2</sup> under four different CEPs, as labeled on the upper right corner of each panel. The two rows are obtained with the same laser parameters except the pulse duration. The laser ellipticity and wavelength are 0.18 and 780 nm, respectively. The ensemble size is  $4 \times 10^4$  in upper row and  $6 \times 10^4$  in bottom row. The relative contribution from short (S) and long (L) recollision trajectories is displayed on the lower right corner of each panel.

Above we have shown that the relative composition of short and long recollision trajectories can be controlled by changing the ellipticity of the laser field while keeping the pulse duration fixed. The changing of this relative contribution manifests itself on the experimentally measurable e-e correlation spectra. Additionally, it is also obvious to expect that the relative contribution of short and long trajectories can be controlled by changing the pulse duration. This point is confirmed by Fig. 8, which shows the e-e momentum correlation spectra for two different pulse durations (upper row: 6 cycles; bottom row: 4 cycles) while keeping the degree of ellipticity fixed. One can see the striking effect of the pulse duration for all the four CEPs used, as labeled on the upper right corner of each panel. The relative contribution of short and long recollision trajectories is shown on the lower right corner of each panel. For the 6-cycle cases (upper row), the short trajectories are found to contribute slightly more than the long trajectories do (about 55% versus 45%); whereas for the 4-cycle cases (bottom row), the short trajectory contribution increases to about 75% due to the substantial suppression of long trajectories. Therefore we see that changing the laser pulse duration is another effective, and experimentally verifiable method, to study the transition of recollision dynamics in double ionization. We comment that this point has also been extensively discussed in Ref [12].

#### 4. Conclusion

In conclusion, we report a theoretical study of recollision mechanism and the resulting NSDI with both linear and elliptical polarization. Previously it has been reported that recollision is dominated by short trajectories for LP and by long trajectories for EP with large ellipticity [12, 13], and this study focuses for the first time on the “intermediate” zone by explaining how exactly the recollision process transitions from short-trajectory-dominant LP to long-trajectory-dominant EP.

We predict that this transition of recollision mechanism leaves its footprints on electron correlation momentum spectra and can be directly observed experimentally using few-cycle, carrier-envelope-phase-stabilized laser pulses, which are available in many laboratories. A detailed statistical and theoretical analysis has also been provided to explain the simulated

electron correlation momentum spectra. We show that the relative contribution of short and long recollision trajectories can be controlled either by changing the field ellipticity or by changing the laser pulse duration.

### **Acknowledgments**

This work was supported by the National Natural Science Foundation of China (Grant Nos. 11134005, 21403144, 11464038, 11404105, 61475132 and 61575169), the National Key Projects for Basic Research of China (Grant Nos. 2015CB921203 and 2013CB922103), the PAPD project, and the Scientific Research Foundation of Education Department of Henan Province of China under Grant Nos. 15A140036. We are also grateful to the High Performance Computing Center of Nanjing University for doing the numerical calculations in this work on its IBM Blade cluster system. Xu Wang was partially supported by Chemical Sciences, Geosciences and Biosciences Division, Office of Basic Energy Sciences, Office of Science, U. S. Department of Energy under Grant No. DE-FG02-86ER13491.